PERGAMON

International Journal of Heat and Mass Transfer 43 (2000) 1233–1242

International Journal of HEAT and MASS TRANSFER

www.elsevier.com/locate/ijhmt

A new angular discretization scheme of the finite volume method for 3-D radiative heat transfer in absorbing, emitting and anisotropically scattering media

Seung Hyun Kim [1], Kang Y. Huh*

Departmeent of Mechanical Engineering, Pohang University of Science and Technology, Pohang, Kyungbuk 790-784, South Korea

Received 20 November 1998; received in revised form 23 April 1999

Abstract

This paper presents a new angular discretization scheme, FT_n, of the finite volume method (FVM) in three-dimensional radiative heat transfer. The FT_n FVM is applied to absorbing, emitting and anisotropically scattering media with variable optical thickness in a rectangular enclosure. Results show that the FT_n FVM performs better than the discrete ordinate method (DOM) and the FVM with $N_\theta \times N_\phi$ uniform angular discretization except near the optically thick diffusion limit. The FT_n FVM closely reproduces the reference solutions by the Monte Carlo method for different scattering phase functions and optical thicknesses. It also turns out that anisotropic scattering has significant influence on radiative heat transfer with a symmetric boundary condition in a moderate optical thickness range as well as with a nonsymmetric boundary condition.

1. Introduction

During the last decade there were numerous efforts to develop suitable numerical schemes for the radiative transfer equation (RTE) [1]. For the problems combined with convective heat transfer or turbulent reacting flows the scheme should be compatible with those for the mass, momentum and energy conservation equations governing the flow field. Implementation of inhomogeneity and anisotropic radiative scattering is required for practical applications in a multidimensional geometry. Among them the FVM has been considered one of the promising schemes for radiative heat transfer with participating media. Since the work of Raithby and Chui [2] the FVM has been extended and applied to various radiative heat transfer problems. Chai et al. [3] presented the results in two- and three-dimensional enclosures with participating media, collimated incidence and heat generation. Chui et al. [4] presented applications to cylindrical geometry and the mapping for a two-dimensional axisymmetric problem in terms of the radiation intensity in the azimuthal direction. The formulations of the FVM for a nonorthogonal grid [5,6] and an unstructured mesh [7] were also presented.

The discrete ordinate method (DOM) replaces the integro differential RTE by a set of coupled differential equations in the discrete ordinate directions. Integration over the solid angle is replaced by a quadrature sum, which is a set of the discrete ordinate directions and the corresponding weights. Although

* Corresponding author. Tel.: +82-562-279-2177; fax: +82-562-279-3199.

E-mail addresses: shk@ace.postech.ac.kr (S.H. Kim), huh@vision.postech.ac.kr (K.Y. Huh).

[1] Tel.: +82-562-279-2841; fax: +82-562-279-3199.

0017-9310/00/$ - see front matter
PII: S0017-9310(99)00211-2

Nomenclature

A	area
a	weighting factor in the temperature distribution
C_m	coefficient in Legendre series
D	direction cosine integrated over the solid angle
e	unit direction vector
f	weighting factor in the spatial discretization scheme
G	incident radiation
I	radiation intensity
k	absorption coefficient
L	length
N	total number of angular discretization
N_θ, N_ϕ	number of angular discretization in the polar and the azimuthal angle
n	unit vector normal to a surface
P_m	Legendre polynomial
Q	radiative heat flux
r	position vector
s	unit vector in the direction of radiation intensity
S	source term in the RTE
T	temperature
V	volume
X, Y, Z	space coordinates

Greek symbols

β	extinction coefficient
ϵ	emissivity
ρ	reflectivity
σ	Stefan–Boltzmann constant
σ_s	scattering coefficient
Φ	scattering phase function
Ω	solid angle
ω	scattering albedo

Subscripts

b	blackbody
P	control volume index
w	wall
X, Y, Z	directions of X, Y and Z
x, y, z	surface elements perpendicular to the directions, X, Y and Z
0	reference quantity

Superscripts

e	exact value
l	control angle index
n	iteration number
$'$	incoming direction
$*$	nondimensional quantity

choice of the quadrature set may be arbitrary, accuracy of the DOM strongly depends on the quadrature set [8,9]. On the other hand discretization of the FVM is based on the same control volume technique as used in computational fluid dynamics. The RTE is integrated over both a discretized control volume and a control angle, so that the discretized equation may describe conservation of radiative energy within each control volume and control angle. Angular discretization of the FVM may be flexible as long as it properly calculates the radiative heat flux and the incident radiation. A common form is the uniform angular discretization in which the polar and the azimuthal angles are both uniformly subdivided. Chai et al. [3] tried nonuniform angular discretization to the problem of collimated incidence by concentrating the angular grid near the direction of the collimated incidence.

There have been several works reported on participating media with anisotropic scattering in a multidimensional geometry. Kim and Lee [10,11] investigated the effect of anisotropic scattering in a two-dimensional rectangular enclosure by the DOM. Similar work was reported in an axisymmetric geometry by Jendoubi et al. [12]. Menguc and Viskanta [13] presented three-dimensional results with the delta-Eddington scattering phase function by the P_3 spherical harmonic method. Fiveland [14] and Truelove [15] reported the results for the same case with Menguc et al. [13] by the DOM. Chui et al. [4] presented the results by the FVM with the delta-Eddington scattering phase function in an axisymmetric problem. Chai et al. [3] and Kim and Baek [16] presented the results in a two-dimensional and an axisymmetric geometry respectively and compared them with those by Kim and Lee [10,11] and Jendoubi et al. [12]. However more validation works are currently required for anisotropic scattering problems with general scattering phase functions in a three-dimensional geometry. Here the FT_n FVM is applied to a three-dimensional rectangular enclosure with anisotropically scattering media with its results validated against the reference solutions by the Monte Carlo method.

2. Finite volume method for radiative transfer

2.1. Radiative transfer equation

The RTE for absorbing, emitting and scattering media is written as

$$(\mathbf{s}\cdot\nabla)I(\mathbf{r},\mathbf{s}) = -(k+\sigma_s)I(\mathbf{r},\mathbf{s}) + kI_b(\mathbf{r}) + \frac{\sigma_s}{4\pi}\int_{4\pi} I(\mathbf{r},\mathbf{s}')\Phi(\mathbf{s}',\mathbf{s})\,d\Omega' \quad (1)$$

where $I(\mathbf{r},\mathbf{s})$ is the radiation intensity in the direction, $\mathbf{s}$, at the position, $\mathbf{r}$. $I_b(\mathbf{r})$ is the blackbody radiation intensity. k and σ_s are the absorption and the scattering coefficient respectively. $\Phi(\mathbf{s}',\mathbf{s})$ is the scattering phase function, which is the fraction of radiative energy scattered into the outgoing direction, $\mathbf{s}$, from the incoming direction, $\mathbf{s}'$. The scattering phase function may be approximated by the Legendre series as

$$\Phi(\mathbf{s}',\mathbf{s}) = \sum_{m=0}^{M} C_m P_m(\mathbf{s}'\cdot\mathbf{s}). \quad (2)$$

The boundary condition on the gray diffuse wall with the prescribed temperature is given as

$$I_w(\mathbf{s}) = \epsilon_w I_{bw} + \frac{1-\epsilon_w}{\pi}\int_{\mathbf{s}'\cdot\mathbf{n}_w<0} I_w(\mathbf{s})|\mathbf{s}'\cdot\mathbf{n}_w|\,d\Omega', \quad (3)$$

where $I_w(\mathbf{s})$ is the radiation intensity on the wall. I_{bw} and ϵ_w are the blackbody radiation intensity and the emissivity of the wall. $\mathbf{n}_w$ is the unit normal vector toward the inside of the enclosure. The incident radiation and the radiative heat flux are given as

$$G(\mathbf{r}) = \int_{4\pi} I(\mathbf{r},\mathbf{s})\,d\Omega \quad (4)$$

$$Q_i(\mathbf{r}) = \int_{4\pi} (\mathbf{e}_i\cdot\mathbf{s})I(\mathbf{r},\mathbf{s})\,d\Omega, \quad (5)$$

where the subscript, i, represents the coordinate directions, X, Y and Z, in Fig. 1. $\mathbf{e}_i$ is the unit vector in the direction i.

2.2. Discretized equation

Integration of Eq. (1) over the control volume, V_P, and the control angle, Ω^l, gives

$$\int_{\Omega^l}\int_{A_P} I(\mathbf{r},\mathbf{s})(\mathbf{s}\cdot\mathbf{n})\,dA\,d\Omega = \int_{\Omega^l}\int_{V_P}(-\beta I(\mathbf{r},\mathbf{s}) + S(\mathbf{r},\mathbf{s}))\,dV\,d\Omega, \quad (6)$$

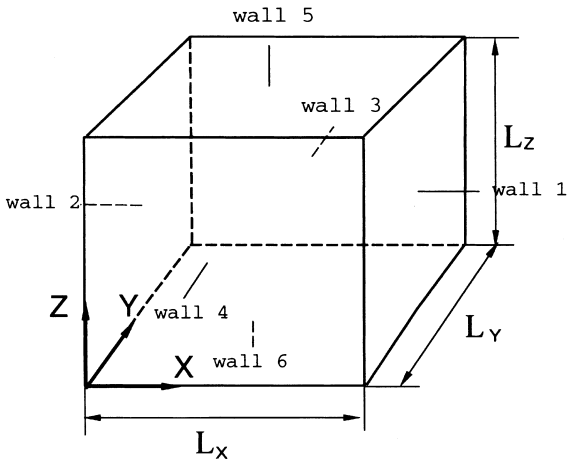

Fig. 1. Geometry of the rectangular enclosure.

where $\beta = k+\sigma_s$ and

$$S(\mathbf{r},\mathbf{s}) = kI_b(\mathbf{r}) + (\sigma_s/4\pi)\int_{4\pi} I(\mathbf{r},\mathbf{s}')\Phi(\mathbf{s}',\mathbf{s})\,d\Omega'.$$

In an orthogonal grid Eq. (6) may be discretized as follows. Treatment of the scattering term is according to Chai et al. [17].

$$A_x|D_X^l|(I_{xu}^l - I_{xd}^l) + A_y|D_Y^l|(I_{yu}^l - I_{yd}^l) + A_z|D_Z^l|(I_{zu}^l - I_{zd}^l) = (-\beta_m^l I_P^l + S_{m,P}^l)V_P\Omega^l, \quad (7)$$

where $\beta_m^l = \beta - (\sigma_s/4\pi)\overline{\Phi^{ll}}\Omega^l$; $S_{m,P}^l = kI_{b,P} + (\sigma_s/4\pi)\sum_{l'\neq l} I_P^{l'}\overline{\Phi^{l'l}}\Omega^{l'}$; $A_x = \Delta Y\Delta Z$, $A_y = \Delta Z\Delta X$, $A_z = \Delta X\Delta Y$, $V_P = \Delta X\Delta Y\Delta Z$; $D_X^l = \int_{\Omega^l}(\mathbf{s}\cdot\mathbf{e}_X)\,d\Omega$, $D_Y^l = \int_{\Omega^l}(\mathbf{s}\cdot\mathbf{e}_Y)\,d\Omega$, $D_Z^l = \int_{\Omega^l}(\mathbf{s}\cdot\mathbf{e}_Z)\,d\Omega$; $\Omega^l = \int_{\Omega^l} d\Omega$ and $\overline{\Phi^{l'l}} = \int_{\Omega^{l'}}\int_{\Omega^l}\Phi(\mathbf{s}',\mathbf{s})\,d\Omega\,d\Omega'/\Omega^{l'}\Omega^l$.

I_{xd}^l, I_{yd}^l and I_{zd}^l are the radiation intensities on the downstream surfaces in the direction, $\mathbf{s}^l$. I_{xu}^l, I_{yu}^l and I_{zu}^l are those on the upstream surfaces in the direction, $\mathbf{s}^l$. The subscripts, x, y and z, denote the surface elements perpendicular to the directions, X, Y and Z, respectively. A weighted finite differencing scheme is used to relate the radiation intensities on cell surfaces with those at cell centers as

$$I_P^l = f_j^l I_{jd}^l + (1-f_j^l)I_{ju}^l, \quad (8)$$

where f_j^l is a weighting factor between 0.5 and 1. The subscript, j, denotes the surface elements, x, y and z. The finite differencing scheme with $f_j^l = 0.5$ is the diamond scheme of the second order accuracy, while the one with $f_j^l > 0.5$ is of the first order accuracy. The

finite differencing scheme with $f_j^l < 1$ does not guarantee a positive value of the radiation intensity. Only the step scheme with $f_j^l = 1$ ensures positivity, although it suffers from numerical diffusion. Lathrop [18] proposed a scheme which guarantees positivity of the radiation intensity with the weighting factors given in terms of the spatial and angular grid. Here a positive scheme is derived in three dimensions according to the procedure of Lathrop [18] as

$$f_x^l = \max\left(1 - \frac{A_x|D_X^l|}{2(A_y|D_Y^l| + A_z|D_Z^l|) + \beta_m^l V_P \Omega^l}, 0.5\right) \tag{9a}$$

$$f_y^l = \max\left(1 - \frac{A_y|D_Y^l|}{2(A_z|D_Z^l| + A_x|D_X^l|) + \beta_m^l V_P \Omega^l}, 0.5\right) \tag{9b}$$

$$f_z^l = \max\left(1 - \frac{A_z|D_Z^l|}{2(A_x|D_X^l| + A_y|D_Y^l|) + \beta_m^l V_P \Omega^l}, 0.5\right). \tag{9c}$$

Eq. (7) can be rearranged with Eqs. (9a)–(9c) as

$$a_P^l I_P^l = a_x^l I_{xu}^l + a_y^l I_{yu}^l + a_z^l I_{zu}^l + b_P^l, \tag{10}$$

where $a_P^l = A_x|D_X^l|/f_x^l + A_y|D_Y^l|/f_y^l + A_z|D_Z^l|/f_z^l + \beta_m^l V_P \Omega^l$; $a_x^l = A_x|D_X^l|/f_x^l$; $a_y^l = A_y|D_Y^l|/f_y^l$; $a_z^l = A_z|D_Z^l|/f_z^l$ and $b_P^l = S_{m,P}^l V_P \Omega^l$.

The boundary condition for Eq. (10) is given as

$$I_w^l = \epsilon_w I_{bw} + \frac{1-\epsilon_w}{\pi} \sum_{D_w^{l'} < 0} I_w^{l'} |D_w^{l'}|, \tag{11}$$

where $D_w^{l'} = \int_{\Omega'} (\mathbf{n}_w \cdot \mathbf{s}')\, d\Omega'$.

Solution of Eq. (10) is an iterative procedure, since the radiation intensities in different control angles are coupled through the source term, $S_{m,P}^l$, and the boundary condition. The radiation intensity in each control angle is obtained by an explicit marching sequence in space. The incident radiation and the radiative heat flux are obtained as

$$G_P = \sum_{l=1}^{N} I_P^l \Omega^l \tag{12}$$

$$Q_{i,r} = \sum_{l=1}^{N} I_r^l D_i^l \tag{13}$$

where the subscript, r, represents the location of evaluation. The detailed solution procedure may be found elsewhere [14,19].

2.3. A new angular discretization scheme

The FVM may adopt any angular discretization scheme that divides the 4π steradian solid angle into an arbitrary number of control angles. It satisfies the zeroth and the first moment, i.e. properly calculates the incident radiation and the radiative heat flux, with uniform radiation intensity in all directions. In an orthogonal grid it allows straightforward calculation of the half range radiative heat flux, which is usually required to implement the boundary condition on the wall. Chui et al. [5] and Murthy et al. [7] presented the procedure to calculate the half range flux in a nonorthogonal grid and an unstructured mesh. The DOM may have some difficulties in a nonorthogonal grid since the quadrature set of the DOM is designed to meet the half range first moment only in an orthogonal grid [8,9].

In the $N_\theta \times N_\phi$ uniform angular discretization scheme of the FVM the polar and the azimuthal angles are uniformly subdivided into N_θ and N_ϕ respectively with the total of $N_\theta \times N_\phi$ control angles. It has been successfully applied to one- and two-dimensional problems [2,3], and gives the mapping for an axisymmetric problem in terms of the radiation intensity in the azimuthal direction [4]. Although it may be simple, it results in highly nonuniform solid angles discretized in three dimensions. Due to overall computational load, efficient angular discretization is more important in three-dimensional problems than in one- and two-dimensional ones. Kim and Huh [19] reported that solution of the FVM with $N_\theta \times N_\phi$ uniform angular discretization may depend on the coordinate system due to nonsymmetric angular discretization in three dimensions.

Here a new angular discretization scheme denoted as FT_n FVM is introduced. The polar angle is divided uniformly into an even number, n, while the azimuthal angle is uniformly divided into the numbers of the sequence of 4, 8, 12,…$2n-4$, $2n$, $2n$, $2n-4$,…8 and 4 in each level of the polar angle as shown in Fig. 2. The increment should be a multiple of 4 to satisfy the half range flux condition. The total number of the control angles, N, is therefore given as $n(n+2)$, which is same as the number of the discrete ordinate directions of the S_n DOM. As shown in Fig. 3 the FT_n FVM results in much more uniform distribution of the discretized control angles in comparison with the FVM with $N_\theta \times N_\phi$ uniform angular discretization. The FT_n FVM satisfies the zeroth moment, the first moment and the half range flux condition in an orthogonal grid.

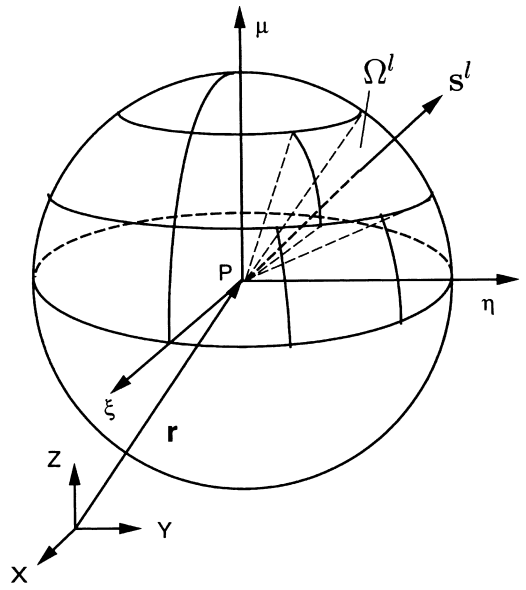

Fig. 2. Angular discretization scheme of the FT_n FVM (Ω^l: solid angle of the lth element, $\mathbf{s}^l$: unit direction vector corresponding to Ω^l).

3. Test cases

The following test cases are defined for the three-dimensional rectangular enclosure shown in Fig. 1. The enclosure is filled with gray, absorbing, emitting and scattering media with gray and diffuse walls. Results are given in nondimensional quantities such as $Q_i^* = Q_i/\sigma T_0^4$ and $G^* = G/4\sigma T_0^4$, where T_0 is the reference temperature. The optical coefficients, k, σ_s and β, are nondimensionalized as $k^* = kL_0$, $\sigma_s^* = \sigma_s L_0$ and $\beta^* = \beta L_0$. The scattering phase functions used in the anisotropic scattering problems are those given by Kim et al. [10] and shown in Fig. 4. The F1 and F2 are the forward scattering phase functions while the B1 and B2 are the backward scattering ones. Convergence of the solution is checked by the condition

$$\max\left(\frac{|G_P^n - G_P^{n-1}|}{G_P^n}\right) < 10^{-5}, \tag{14}$$

where the superscript, n, is an iteration number.

3.1. Purely absorbing/emitting medium

The enclosure with black and cold walls at 0 K is filled with purely absorbing/emitting medium with the temperature distribution given as

$$\begin{aligned} T(X,Y,Z) &= aT_0(1-r^2)(1-p^2) + (1-a)T_0, \\ r &= \sqrt{2}[(Y/L_0 - 1/2)^2 + (Z/L_0 - 1/2)^2]^{1/2} \\ p &= 2X/L_X - 1, \end{aligned} \tag{15}$$

where a is the weighting factor to describe nonuniformity of the temperature distribution. L_0 is the characteristic length equal to L_Y and L_Z. The parabolic profile in Eq. (15) has the maximum value, T_0, at the center of the enclosure and the minimum value, $(1-a)T_0$, on all the edges and the walls 1 and 2. Here the RTE becomes a first order differential equation with no coupling among different propagating directions and may be integrated as

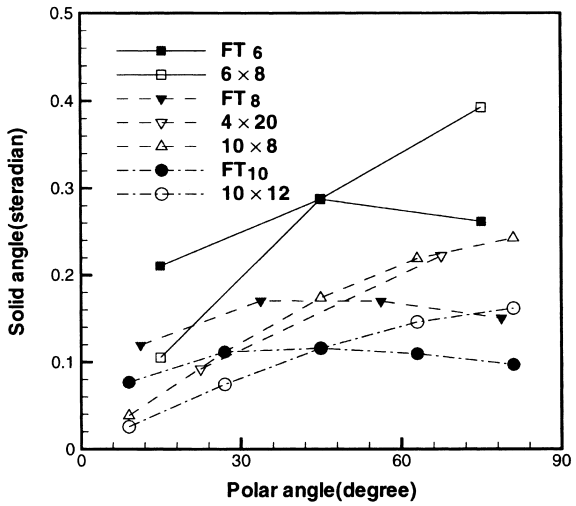

Fig. 3. Comparison of the discretized solid angles between the FT_n FVM and the $N_\theta \times N_\phi$ FVM.

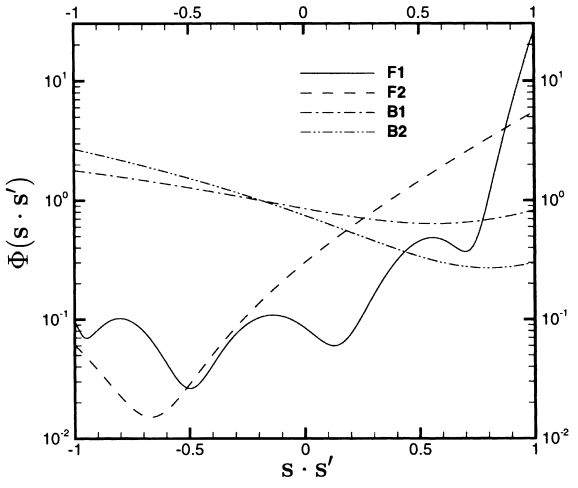

Fig. 4. Scattering phase functions by the Legendre series (F1 and F2: forward scattering phase functions, B1 and B2: backward scattering phase functions).

$$I(\mathbf{r},\mathbf{s}) = k\int_0^s I_b(\mathbf{r}-v\mathbf{s})e^{-kv}\,dv, \tag{16}$$

where s is the distance in the direction, $\mathbf{s}$, from the wall. The exact solutions for the radiative heat flux are obtained by numerical integration of Eqs. (5) and (16). The solutions of the FVM and DOM are obtained with the radiation intensity given by Eq. (16) to investigate accuracy of the angular discretization schemes without the error due to spatial discretization.

3.2. Ideal furnace

This ideal furnace has already been studied by several investigators [3,13–15]. It has a uniform heat source, $\dot{q}=5$ kW/m^3, and is filled with absorbing and emitting media. The absorption coefficient, k, is 0.5 m^{-1}. Its geometry and boundary conditions are given as follows.

$L_X=2$ m $L_Y=2$ m $L_Z=4$ m at $Z=0$,
$T=1200$ K $\epsilon_w=0.85$, at $Z=L$,
$T=400$ K $\epsilon_w=0.70$,
otherwise $T=900$ K $\epsilon_w=0.70$.

Since the RTE is coupled with the energy equation given as

$$\dot{q} = k\left(4\pi I_b(\mathbf{r}) - \int_{4\pi} I(\mathbf{r},\mathbf{s})\,d\Omega\right), \tag{17}$$

the solution is obtained by substituting Eq. (17) into Eq. (1). The furnace is divided into $25\times25\times25$ control volumes.

3.3. Anisotropic scattering problems

3.3.1. Purely scattering medium with diffuse incidence — nonsymmetric boundary condition

Radiative energy is emitted only from wall 6 and transferred, through purely scattering medium, to the other walls. The enclosure is cubical with the side length, L_0. The scattering coefficient, σ_s^*, is equal to one. The temperature of wall 6 is T_0 while the temperature of the other walls is 0 K. All the walls of the enclosure are black. The enclosure is divided into $25\times25\times25$ control volumes. The results are compared with the Monte Carlo solutions [1,20], which are obtained by dividing wall 6 into 25×25 subsurfaces and emitting 10^6 energy bundles from each subsurface.

3.3.2. Isothermal medium with cold diffuse walls — symmetric boundary condition

The cubical enclosure with the side length, L_0, is filled with the isothermal medium at the temperature, T_0, which absorbs, emits and scatters anisotropically. The walls of the enclosure are cold at 0 K and black except for the case in Fig. 9. The enclosure is divided into $25\times25\times25$ control volumes. The Monte Carlo solutions are obtained by dividing the enclosure into $15\times15\times15$ subvolumes and emitting 10^6 energy bundles for β^* equal to 1 and 2 and 3×10^6 energy bundles for β^* equal to 10 from each subvolume.

4. Results

4.1. Purely absorbing/emitting medium

Table 1 lists the average relative errors of the FT_n FVM, $N_\theta\times N_\phi$ FVM and S_n DOM for varying optical thickness, temperature profile and aspect ratio. The average relative error is defined as

$$\epsilon = \frac{1}{P}\sum_r \frac{|Q_{Z,r}-Q^e_{Z,r}|}{Q^e_{Z,r}}, \tag{18}$$

where P is the total number of the evaluation locations. $Q^e_{Z,r}$ is the exact solution at the location, r. N_θ and N_ϕ are equal to $2n_\theta$ and $4n_\phi$, where n_θ and n_ϕ are positive integers. Note that the FT_n FVM is the most accurate in most cases in Table 1 except in the optically thick diffusion limit. The FVMs are more accurate than the S_n DOM except in the optically thick case of k^* equal to 10. In the optically thick diffusion limit the radiation intensity may be approximated as the sum of the incident radiation and the radiative heat flux vector projected into the direction vector, $\mathbf{s}$. The FVM in general does not satisfy the second moment condition given as

$$\sum_{l=1}^{N}\left(\frac{D_i^l}{\Omega^l}\right)^2\Omega^l = \frac{4}{3}\pi, \tag{19}$$

where the subscript, i, denotes the coordinate directions, X, Y and Z [8,9]. The quadrature set of the S_n DOM, higher than S_4, is designed to meet this condition in the diffusion limit.

4.2. Ideal furnace

Figure 5 shows the radiative heat flux on walls 5 and 6 of the ideal furnace. The solutions of the FT_n FVM are compared with those of the 4×20 FVM, the S_8 DOM and the zone method. The results of the zone method and the S_8 DOM are taken from Truelove [15] and Fiveland [14] respectively. The FT_8 FVM and S_8 DOM show comparable accuracy with their solutions close to those of the zone method. The FT_6 FVM gives a more accurate solution than the 4×20 FVM, although the number of angular discretization of the FT_6 FVM is less than that of 4×20 FVM. The 4×20

Table 1
Average relative errors for the nondimensional radiative heat flux with purely absorbing/emitting media in a rectangular enclosure

Scheme	Total number of angular discretization	L_X/L_0	Errors (%)					
			$a = 0.5$			$a = 1$		
			$k^* = 0.1$	$k^* = 1$	$k^* = 10$	$k^* = 0.1$	$k^* = 1$	$k^* = 10$
FT_4 FVM	24	1	1.808	1.280	2.055	5.984	5.581	9.625
FT_6 FVM	48		0.376	0.559	0.896	0.738	1.289	3.817
FT_8 FVM	80		0.581	0.358	0.489	0.319	0.285	2.192
2×12 FVM	24		20.177	17.170	5.817	37.845	35.217	18.589
4×12 FVM	48		2.563	3.146	2.132	5.623	6.546	7.793
6×8 FVM	48		1.260	0.843	0.891	2.507	2.214	3.420
4×20 FVM	80		2.864	3.406	2.164	6.124	6.941	7.651
10×8 FVM	80		1.488	0.879	0.262	1.778	1.176	1.555
S_4 DOM	24		7.438	5.832	0.742	18.300	16.530	8.026
S_6 DOM	48		2.842	1.880	0.156	7.007	6.358	2.666
S_8 DOM	80		1.977	1.396	0.053	6.067	5.236	1.224
FT_4 FVM	24	3	2.040	1.694	1.847	16.906	14.768	8.678
FT_6 FVM	48		0.561	0.388	0.815	6.673	5.610	3.651
FT_8 FVM	80		0.663	0.124	0.453	2.308	1.907	2.051
2×12 FVM	24		9.392	8.394	5.534	32.761	30.217	19.792
4×12 FVM	48		3.031	2.160	2.001	6.664	6.323	7.647
6×8 FVM	48		2.549	1.220	0.815	12.973	9.719	3.602
4×20 FVM	80		3.783	2.549	2.037	11.505	8.435	7.565
10×8 FVM	80		2.285	0.926	0.227	10.507	7.179	1.556
S_4 DOM	24		2.285	1.747	0.222	12.823	11.309	4.594
S_6 DOM	48		2.039	1.418	0.044	6.964	7.309	1.972
S_8 DOM	80		4.572	2.746	0.017	9.166	7.378	0.983

FVM was previously used by Chai et al. [3] for the same case.

The FT_6 and FT_8 FVMs needed 13 and 14 iterations respectively to reach a converged solution satisfying the criterion in Eq. (14). The 4×20 FVM needed the same number of iterations as the FT_8 FVM.

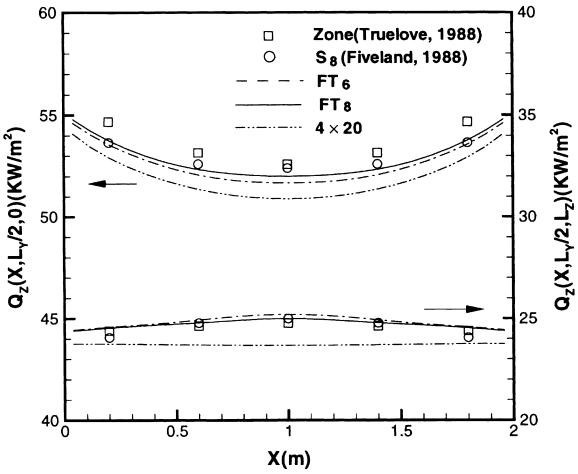

Fig. 5. Radiative heat fluxes on the walls of the ideal furnace.

4.3. Anisotropic scattering problems

4.3.1. Purely scattering medium with diffuse incidence — nonsymmetric boundary condition

Figure 6 shows the radiative heat flux, Q_Z^*, along the centerline of the enclosure, ($L_0/2$, $L_0/2$, Z), with isotropic scattering. Note that the solutions of the FT_8 FVM and S_8 DOM show some oscillation due to the inaccuracy in angular approximation. The results of the 10×12, and FT_{10} FVMs are close to the Monte Carlo solution in Fig. 6. Pessoa-Filho and Thynell [22] reported that discontinuity in the radiation intensity exists in the angular domain for a similar two-dimensional case obtained by increasing the aspect ratio, L_X/L_0, to infinity. Discontinuity in the radiation intensity may exist not only on the wall but also inside the enclosure when a highly nonsymmetric boundary condition is imposed. The ray effect tends to become more pronounced when there is discontinuity or a sharp change in the radiation intensity in the angular domain [21,22].

Figure 7 shows the effect of anisotropic scattering

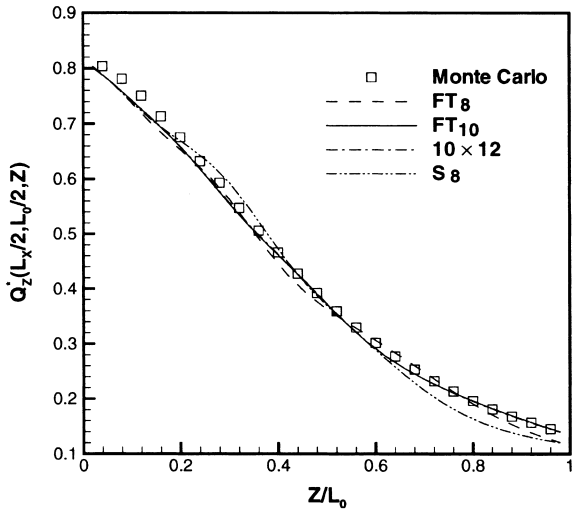

Fig. 6. Nondimensional radiative heat flux for purely scattering medium with isotropic scattering subject to diffuse radiation from wall 6 of the cubical enclosure ($\sigma_s^*=1$, $\omega=1$).

on the radiative heat flux. The radiative heat flux, Q_Z^*, is obtained by the FT_{10} FVM and the Monte Carlo method for different scattering phase functions. Note that the results of the FT_{10} FVM closely follow the Monte Carlo solutions for all the scattering phase functions considered. The forward scattering media with the phase functions, F1 and F2, transfer more radiative energy through the medium than the isotropic and the backward scattering media with the phase functions, B1 and B2. As the aspect ratio, L_X/L_0, increases, the solution approaches the two-dimensional solutions by Kim and Lee [10] and Pessoa-Filho and Thynell [22].

4.3.2. Isothermal medium with cold diffuse walls — symmetric boundary condition

Figure 8 shows the radiative heat flux, Q_Z^*, along the line, (X, $L_0/2$, L_0), with isotropic scattering. The extinction coefficient, β^*, and the scattering albedo, $\omega=\sigma^*/\beta^*$, are 1 and 0.5 respectively. The results of the FT_6 and FT_8 FVMs are compared with those of the Monte Carlo method, the 10×8 FVM and the S_8 DOM. The FT_8 FVM gives the most accurate solution in agreement with the reference solution by the Monte Carlo method. Note that all the FVMs give more accurate solutions than the S_8 DOM in Fig. 8.

Figure 9 shows the incident radiation along the line, (X, $L_0/2$, $L_0/2$), for different scattering phase functions and two wall reflectivities, 0 and 0.5. The results are obtained by the FT_8 FVM. The walls are cold at 0 K and reflect radiation diffusely. The extinction coefficient, β^*, and the scattering albedo, ω, are 2 and 0.5 respectively. The FT_8 FVM closely reproduces the reference solutions by the Monte Carlo method for all the scattering phase functions and wall reflectivities considered. Note that the incident radiation shows strong dependence on the scattering phase function. The maximum difference occurs at the location of the maximum incident radiation near the center of the enclosure. The forward scattering media give lower incident radiation than the isotropic scattering media, which again give lower incident radiation than the backward scattering media. The backward scattering media tends to block transfer of radiative energy to

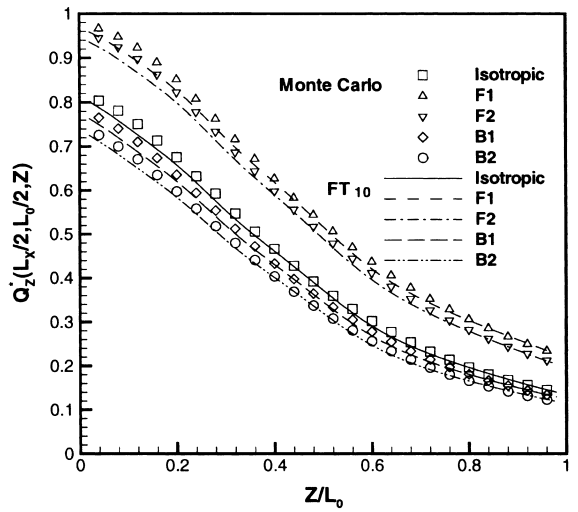

Fig. 7. Effect of anisotropic scattering on the radiative heat flux for purely scattering medium subject to diffuse radiation from wall 6 of the cubical enclosure ($\sigma_s^*=1$, $\omega=1$).

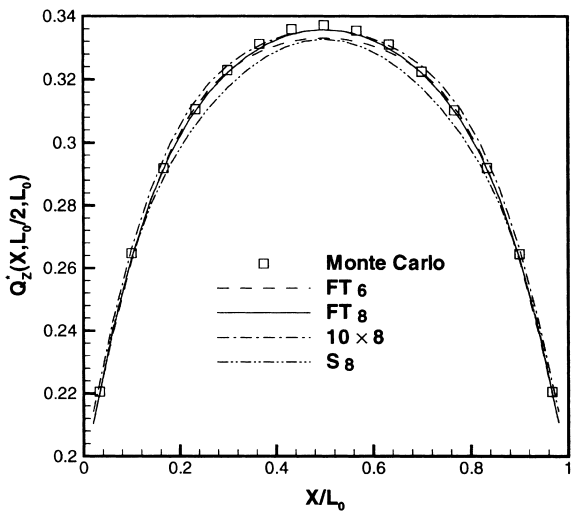

Fig. 8. Nondimensional radiative heat flux for isothermal, isotropically scattering medium in the cubical enclosure with black and cold walls ($\beta^*=1$, $\omega=0.5$).

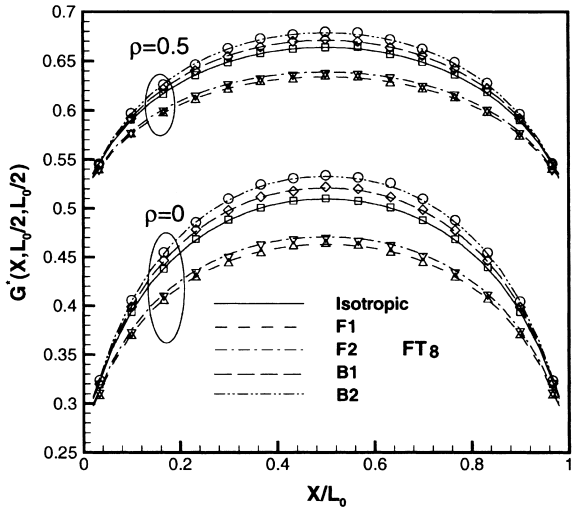

Fig. 9. Effect of anisotropic scattering and wall reflectivity on the incident radiation for isothermal medium in the cubical enclosure with diffuse and cold walls ($\beta^*=2$, $\omega=0.5$, Monte Carlo □: isotropic, △: F1, ▽: F2, ◇: B1, ○: B2).

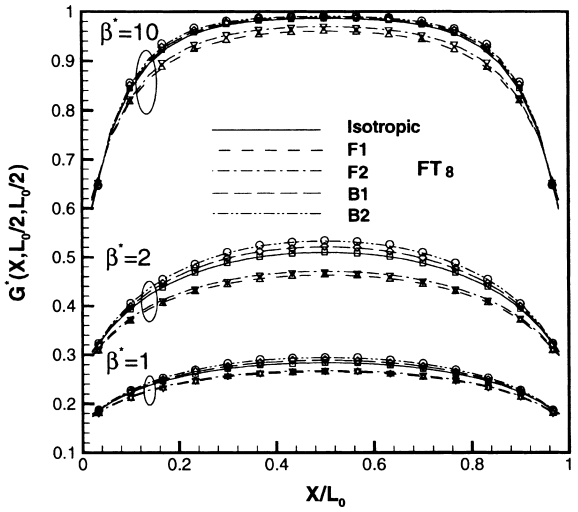

Fig. 11. Effect of anisotropic scattering on the incident radiation for different optical thicknesses ($\omega=0.5$, Monte Carlo □: isotropic, △: F1, ▽: F2, ◇: B1, ○: B2).

the walls and absorb more energy. Note that the incident radiation increases and becomes flatter in space as the reflectivity increases in Fig. 9. The difference among the solutions with different scattering phase functions also decreases as the wall reflectivity increases, because diffuse reflection on the walls tends to compensate for the effect of anisotropic scattering.

Figures 10 and 11 show the effect of anisotropic scattering on the radiative heat flux and incident radiation as the optical thickness varies. The extinction coefficients, β^*, are 1, 2 and 10, while the scattering albedo, ω, is fixed as 0.5. The results are obtained by the FT_8 FVM as in Fig. 9. Figure 10 shows the radiative heat flux, Q_Z^*, along the line, (X, $L_0/2$, L_0). The effect of anisotropic scattering is negligible for β^* equal to 1, since it corresponds to an optically thin case without much scattering occurring. The radiative heat flux shows some variation of different scattering phase functions with β^* equal to 2. The forward scattering media result in the radiative heat fluxes slightly higher than those for the isotropic and backward scattering media. The effect of anisotropic scattering results in significant variation in the radiative heat flux for the extinction coefficient, β^*, equal to 10. Figure 11 shows the incident radiation along the line, (X, $L_0/2$, $L_0/2$). Note that anisotropic scattering affects the incident radiation at lower optical thickness than for the radiative heat flux in Fig. 10. It is because the scattered radiation contributes to increasing the incident radiation, while it may increase or decrease the radiative heat flux according to the propagation direction after scattering. There may be a significant effect of anisotropic scattering for the isothermal media with a symmetric boundary condition and a moderate optical thickness. The effect of anisotropic scattering was reported to be negligible for isothermal media in a two-dimensional rectangular enclosure [10] and axisymmetric geometry [12].

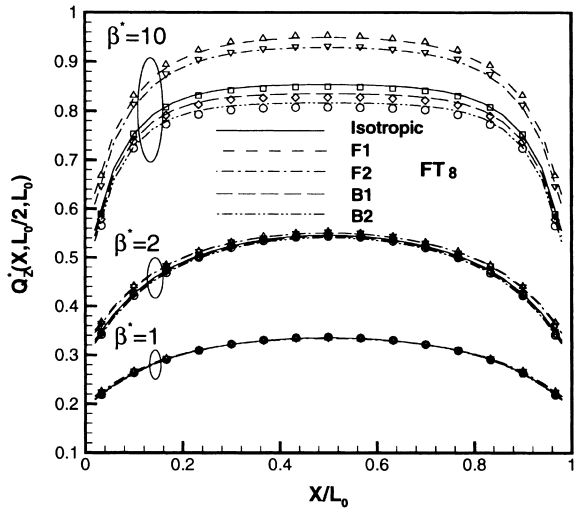

Fig. 10. Effect of anisotropic scattering on the radiative heat flux for different optical thicknesses ($\omega=0.5$, Monte Carlo □: isotropic, △: F1, ▽: F2, ◇: B1, ○: B2).

5. Concluding remarks

The FVM with a new angular discretization scheme,

FT_n FVM, is presented and applied to a three-dimensional rectangular enclosure with absorbing, emitting and anisotropically scattering media. The positive spatial discretization procedure of Lathrop is extended to ensure positive radiation intensity in three dimensions. Results show that the FT_n FVM gives a more accurate solution than the DOM and the FVM with $N_\theta \times N_\phi$ uniform angular discretization with the same total number of angular discretization except in the optically thick diffusion limit. It is because the FVM does not satisfy the second moment condition to be an accurate formulation in the diffusion limit. The FT_n FVM reduces the ray effect and the error due to nonsymmetric angular discretization under rotation of the axes in three dimensions. The effect of anisotropic scattering is also investigated with the scattering phase functions given by the finite series Legendre polynomials. The solutions of the FT_n FVM show good agreement with the reference solutions by the Monte Carlo method for different scattering phase functions and optical thicknesses. Anisotropic scattering has a significant effect not only with a nonsymmetric boundary condition but also in the isothermal media of a moderate optical thickness and scattering albedo with a symmetric boundary condition.

References

[1] M.F. Modest, Radiative Heat Transfer, McGraw-Hill Inc, 1993.

[2] G.D. Raithby, E.H. Chui, A finite-volume method for predicting a radiant heat transfer in enclosures with participating media, ASME J. Heat Transfer 112 (1990) 415–423.

[3] J.C. Chai, H.S. Lee, S.V. Patankar, Finite volume method for radiation heat transfer, J. Thermophys. Heat Transfer 8 (1994) 419–425.

[4] E.H. Chui, G.D. Raithby, P.M.J. Hughes, Prediction of radiative transfer in cylindrical enclosures with the finite volume method, J. Thermophys. Heat Transfer 6 (4) (1992) 605–611.

[5] E.H. Chui, G.D. Raithby, Computation of radiant heat transfer on a nonorthogonal mesh using the finite volume method, Numerical Heat Transfer Pt. B 23 (1993) 269–288.

[6] J.C. Chai, S. Parthasarathy, H.S. Lee, S.V. Patankar. A finite-volume radiation heat transfer procedure for irregular geometries. AIAA Paper 94-2095, June 1994.

[7] J.Y. Murthy, S.R. Mathur, Finite volume method for radiative heat transfer using unstructured meshes, J. Thermophys. Heat Transfer 12 (3) (1998) 313–321.

[8] K.D. Lathrop, B.G. Carlson. Discrete-ordinates angular quadrature of the neutron transport equation. Technical Information Series Report LASL-3186, Los Alamos Scientific Laboratory, (1965).

[9] W.A. Fiveland, The selection of discrete ordinate quadrature sets for anisotropic scattering, Fundam. Radiation Heat Transfer HTD-160 (1991) 89–96.

[10] T.K. Kim, H.S. Lee, Effect of anisotropic scattering on radiative heat transfer in two-dimensional rectangular enclosures, Int. J. Heat Mass Transfer 31 (8) (1988) 1711–1721.

[11] T.K. Kim, H.S. Lee, Radiative heat transfer in two-dimensional anisotropic scattering media with collimated incidence, J. Quant. Spectrosc. Radiat. Transfer 42 (3) (1989) 225–238.

[12] S. Jendoubi, H.S. Lee, T.K. Kim, Discrete ordinates solutions for radiatively participating media in a cylindrical enclosure, J. Thermophys. Heat transfer 7 (1993) 213–219.

[13] M.P. Menguc, R. Viskanta, Radiative transfer in three-dimensional rectangular enclosures containing inhomogeneous, anisotropically scattering media, J. Quant. Spectrosc. Radiat. Transfer 33 (6) (1985) 533–549.

[14] W.A. Fiveland, Three-dimensional radiative heat transfer solutions by the discrete ordinates method, J. Thermophys. Heat Transfer 2 (4) (1988) 309–316.

[15] J.S. Truelove, Three-dimensional radiation in absorbing–emitting–scattering media using the discrete-ordinates approximation, J. Quant. Spectrosc. Radiat. Transfer 39 (1988) 27–31.

[16] M.Y. Kim, S.W. Baek, Analysis of radiative transfer in cylindrical enclosures using the finite volume method, J. Thermophys. Heat Transfer 11 (2) (1997) 246–252.

[17] J.C. Chai, H.S. Lee, S.V. Patankar, Improved treatment of scattering using the discrete ordinates method, ASME J. Heat Transfer 116 (1994) 260–263.

[18] K.D. Lathrop, Spatial differencing of the transport equation: positivity vs. accuracy, J. Computational Phys. 4 (1969) 475–498.

[19] S.H. Kim, K.Y. Huh. Assessment of the finite volume method and the discrete ordinate method in a three-dimensional rectangular enclosure. Numerical Heat Transfer Pt. B 36 (1999) 85–112.

[20] D.V. Walters, R.O. Buckius, in: Monte Carlo methods for radiative heat transfer in scattering media, Annual Review of Heat Transfer, 5, Hemisphere, New York, 1992.

[21] J.C. Chai, H.S. Lee, S.V. Patankar, Ray effect and false scattering in the discrete ordinates method, Numerical Heat Transfer Pt. B 24 (1993) 373–389.

[22] J.B. Pessoa-Filho, S.T. Thynell, An approximate solution to radiative transfer in two-dimensional rectangular enclosures, ASME J. Heat Transfer 119 (1997) 738–745.